EPJ Web of Conferences **233**, 04002 (2020) https://doi.org/10.1051/epjconf/202023304002
CMPNC 2019

Investigating the anisotropic compression and high-pressure phase symmetry of orthorhombic $RFeO_3$ vs $RMnO_3$

R. Vilarinho[1,], A. Almeida[1], and J. Agostinho Moreira[1,*]*

[1]IFIMUP, Physics and Astronomy Department, Faculty of Sciences, University of Porto, Rua do Campo Alegre 687, s/n- 4169-007 Porto, Portugal.

Abstract. Rare-earth orthoferrites and orthomanganites present strong couplings between their structural distortions and physical properties, namely magnetoelectricity, generating interest in predicting and realizing new phases under external parameters, such as hydrostatic pressure. In this regard, we discuss the differences and the similarities of the high-pressure behaviour of the structural distortions arising from anisotropic volume compression. This allows a better understanding of the role played by the octahedra tilt and Jahn-Teller effect as pressure accommodation mechanisms on the stabilization of different crystallographic phases after the insulator to metal structural transition occurring at the critical pressures (P_C) between 35 and 50 GPa.

1 Introduction

The physical properties of perovskite materials, with general formula ABO_3, are known to be strongly dependent on their structural distortions, which can be changed through temperature, applied electric/magnetic fields, and epitaxial strain. The understanding of the delicate energy balance involving the different structural instabilities is therefore a key point for the design of multifunctional perovskite-based materials, and can give important inputs for *ab initio* calculations and phenomenological models [1–3]. Hydrostatic pressure allows modifying the interatomic distances and, thus, tuning the interactions to a much larger extent that any other external parameters. We have amply used this advantage in the past for the understanding of model perovskites [4–6].

Rare-earth orthoferrites ($RFeO_3$), and orthomanganites ($RMnO_3$) (with R lanthanide atom) exhibit interesting magnetic phases. In the $RFeO_3$, ferroelasticity and the predicted ferroelectric properties at room conditions in epitaxial films have renewed the interest for this family of compounds [7,8]. This motivates a better understanding of the compressibilities of these structures. All of $RFeO_3$ and the $RMnO_3$, with R = La to Dy, crystallize at ambient conditions in the *Pnma* space group, characterized by two independent tilts of the oxygen octahedra: the in-phase rotation about the $[010]_{pc}$ axis, and the out-of-phase $[101]_{pc}$ axis. [7]. For the same rare-earth, the $RFeO_3$ and $RMnO_3$ exhibit exactly the same the tolerance factor, as Mn^{3+} and Fe^{3+} have the same ionic radius for the 6th coordination in the high spin configuration. However, the MnO_6 octahedron exhibits

Jahn-Teller distortion, which is superimposed to the intrinsic distortion arising from the out-of-phase $[101]_{pc}$ octahedra tilt.

In order to disclose the effect of the structural distortions referred to above on the physical properties of $RFeO_3$, $RMnO_3$, their high-pressure behaviour has been studied to some extend by x-ray diffraction, Mössbauer spectroscopy, and resistivity measurements [5,6,9–14]. A general scenario can be summarized, wherein both types of compounds undergo compression before a structural phase transition occurs at P_C in the 35 to 50 GPa range, depending on the rare-earth ion. This phase transition, usually of the first-order, with a volume collapse of the order of 5%, is accompanied with an insulator-to-metal transition, which has been explained by a high-spin to low-spin state change of the Fe^{3+} and Mn^{3+} cations by Mössbauer spectroscopy [5,6,9–12].

This work focuses on the similarities and differences found in the high-pressure behaviour of $RFeO_3$ and $RMnO_3$ to evidence the role played by the Jahn-Teller distortion, namely on the degree of anisotropy, volume compression, and symmetry of the high-pressure crystallographic phase.

2 Results and discussion

This part of the work will be mainly based on the experimental results reported by R. Vilarinho et al. for the $RFeO_3$ [6] and by D. Mota et al. for the $RMnO_3$ [5], as they embraced the high-pressure behaviour for a large set of rare-earth ions in these systems. These works were based on the synchrotron x-ray diffraction and Raman scattering techniques. From these experimental results, some physical quantities, which were not presented in the original papers, are now calculated and compared.

2.1 High-pressure phase transition

The insulator-to-metallic phase transition in both $RFeO_3$ and $RMnO_3$ series was revealed by the disappearance of the Raman signature above a certain critical pressure. Simultaneously, changes on the x-ray diffraction patterns are found and on the pressure dependence of the lattice parameters obtained from them. The transition is reversible being both the Raman spectrum and the crystallographic structure recovered upon pressure decreasing, with a significant hysteresis ranging between 3 to 6 GPa depending on the rare-earth cation.

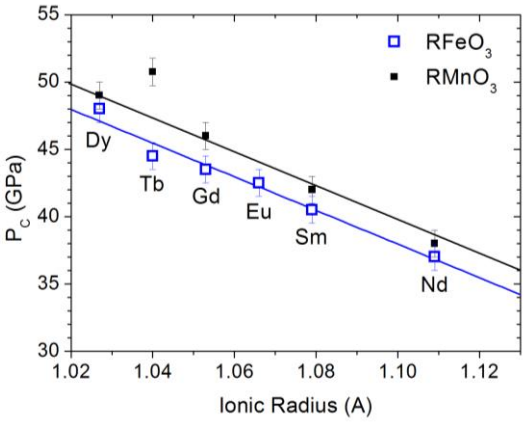

Fig. 1. Critical pressure for $RFeO_3$ (open symbols) and $RMnO_3$ (closed symbols) as a function of the ionic radius for the 6th coordination in the high spin configuration. Data from Refs [5] and [6].

The value for the critical pressure P_C, obtained from the synchrotron x-ray diffraction and Raman scattering data, are depicted in Figure 1 [5,6]. In both cases, as the rare-earth cation size decreases, the critical pressure increases. It is reasonable to assume that, as pressure increases and the FeO_6 octahedra becomes smaller, a critical volume is reached where the electronic repulsion between the oxygen 2p-electrons and the iron e_g-electrons is such, that it is energetically favourable for the latter to pair with the t_{2g}-electrons, avoiding the oxygens 2p-electrons. If we assume this scenario, it is then expectable that for larger R-cations, where FeO_6 octahedra cannot increase their tilts to accommodate the applied pressure, they must reduce their volume and promote the phase transition at a lower critical pressure. Moreover, one can compare these critical pressures with their respective values for the similar pressure-driven phase transition observed in $RMnO_3$ [5]. The critical pressures for $RMnO_3$ are systematically slightly higher than the ones obtained for $RFeO_3$, by an apparent constant value of 2 GPa. This difference can easily be understood using the same logical reasoning as before by taking into account that the Jahn-Teller distortion present in $RMnO_3$ provides an additional pressure accommodation mechanism than in their respective $RFeO_3$ compounds. It is worth to note that the tilt angles for $RFeO_3$ and $RMnO_3$, with the same rare-earth ion, are almost the same, thus allowing for this comparison [15].

Concerning the symmetry of the high-pressure phase, while for $RFeO_3$ it always exhibits the *Pnma* symmetry, no common rule could be ascertained from the experimental results of $RMnO_3$. Though $DyMnO_3$ in fact has an isostructural phase transition at P_C, the best refinements obtained for the high-pressure phase symmetry of $PrMnO_3$ are tetragonal (*I4/mcm*) and of $GdMnO_3$ are cubic ($P2_13$) [5]. For the case of $SmMnO_3$ it is not conclusive, but it appears not to be *Pnma* [5]. Figure 2 shows the symmetries of these crystallographic phases on a bar-plot, both for $RFeO_3$ and $RMnO_3$.

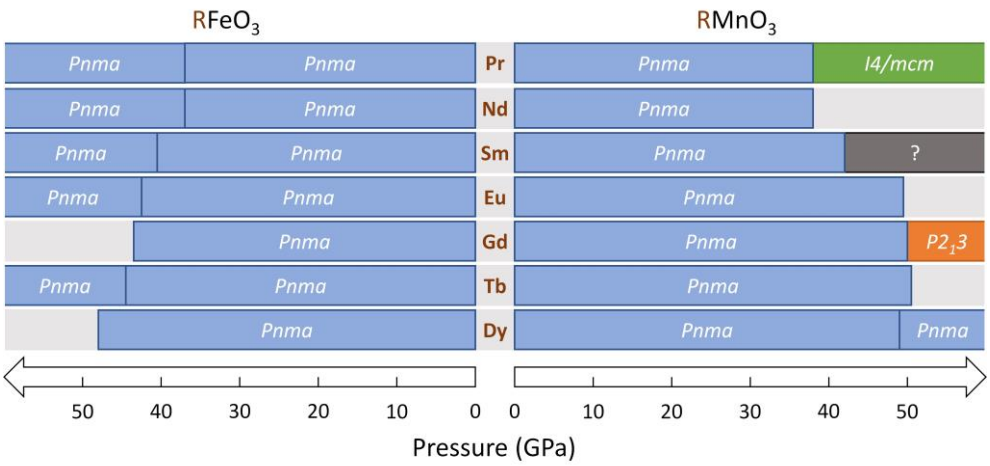

Fig. 2. Symmetry of the crystallographic phases identified in $RFeO_3$ (left) and $RMnO_3$ (right) through x-ray diffraction as a function of applied hydrostatic pressure. Data from Refs. [5,6,9–12].

2.2 Pressure evolution of structural strain

The low quality of the XRD patterns obtained at high pressures has hindered the full Rietveld refinement of the atomic positions and, so, the calculation of the tilt angles. Thus, in order to highlight the role played by the Jahn-Teller distortion and compare on the pressure evolution of the structural distortions below P_C, we have calculated and compared the shear e_4 strain from the lattice parameters for both $RFeO_3$ and $RMnO_3$ [16]:

$$e_4 = [(a_{pc} - a_0) - (c_{pc} - a_0)]/a_0 \,, \qquad (1)$$

where $a_{pc} = a/\sqrt{2}$ and $c_{pc} = c/\sqrt{2}$ are the pseudocubic lattice parameters and $a_0 = \sqrt[3]{V_{pc}}$, with $V_{pc} = a_{pc}xb_{pc}xc_{pc}$. According to Landau theory and symmetry arguments, the symmetry adapted shear e_4 strain provides information regarding primarily the out-of-phase $[101]_{pc}$ octahedra tilt [17].

Figures 3(a) and (b) show the shear e_4 strain as a function of applied pressure for $RFeO_3$ and $RMnO_3$, respectively. For the $RFeO_3$ with rare-earth ions larger than Eu^{3+}, the shear e_4 strain reduces as pressure increases, while it is enlarged for those smaller than Eu^{3+}. $EuFeO_3$ sits exactly at the crossover between these two behaviours, wherein the shear e_4 strain is constant with pressure. This result corroborates the correlation between the shear-strain and the $[101]_{pc}$ octahedra tilt, since the behaviour of the shear-strain with pressure of the $RFeO_3$ exactly mimics that found for the $[101]_{pc}$ octahedra tilt in a previous work [6].

For the $RMnO_3$ a somewhat similar evolution of the pressure dependence of the shear strain on the rare-earth size is found, though the crossover occurs very close to $DyMnO_3$. Thus, for rare-earth ions larger than Dy^{3+}, a reduction of the shear-strain with increasing pressure is observed, while only for $DyMnO_3$ it slightly increases. Two important notes are worth mentioning: i) the rare-earth manganite with the next smaller rare-earth, $HoMnO_3$, is no longer orthorhombic when processed at ambient pressure, and therefore cannot be used for comparison; ii) the $[101]_{pc}$ octahedra tilt cannot be estimated by the lattice parameters alone, as it was done in the $RFeO_3$, due to the higher degree of distortion of the MnO_6 octahedra emerging from the Jahn-Teller effect.

To better elucidate the pressure dependence of the shear strain, Figure 4(a) presents the slopes of the linear pressure-relation of the shear e_4 strain, obtained below 15 GPa, as a function of the rare-earth size for both systems, simultaneously. Although a similar crossover between increasing and decreasing of the shear-strain with increasing pressure is found both in $RFeO_3$ and $RMnO_3$, the evolution of the variation rate with the rare-earth ionic size is much more drastic in the $RMnO_3$, with only $DyMnO_3$ presenting values within those found for $RFeO_3$. From these results we estimate that the crossover between reduction/enhancement of the tilt angles known for $RFeO_3$, not only should also emerge in the $RMnO_3$, but be more pronounced, meaning that the suppression rate of the tilt angles for rare-earth ions larger than Gd^{3+} should be much larger than those found for any of the $RFeO_3$.

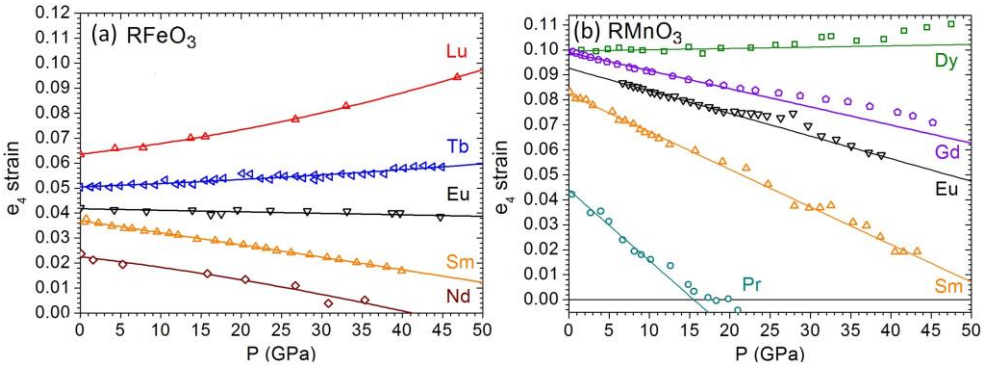

Fig. 3. Shear e_4 strain pressure dependence for (a) $RFeO_3$ and (b) $RMnO_3$. Data of (b) from Ref. [5].

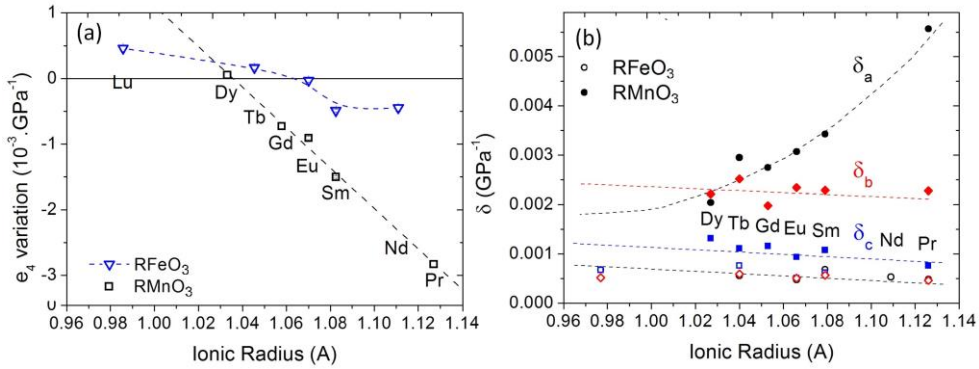

Fig. 4. (a) Shear e_4 strain linear pressure slope and (b) compressibility of lattice parameters for $RFeO_3$ and $RMnO_3$, as a function of rare-earth ionic radius. Data for $RMnO_3$ from Ref. [5].

The apparent change of the shear-strain as pressure increases can be straightforwardly associated to an anisotropic volume reduction. In fact, if the volume reduction was isotropic, the shear-strain would be constant with pressure, as it is the case of $EuFeO_3$. Thus, we have proceeded to calculate the directional compressibilities $\delta_i = 1/(3B^i_0)$, where B^i_0 is the bulk modulus obtained by the best fit of the third-order Birch-Murnaghan equation of state to the lattice parameter *i*. Figure 4(b) presents these compressibilities as a function of the rare-earth ionic radius for both $RFeO_3$ and the $RMnO_3$. In the case of rare-earth orthoferrites (open symbols), the volume reduction is close to isotropic, since the three different compressibilities take the same value. This result agrees with the small variation rates of the shear-strain found for the $RFeO_3$. Conversely, for the rare-earth orthomanganites (closed symbols) this is not the case, where $\delta_a > \delta_b > \delta_c$. The anisotropy of the volume reduction strongly increases as the rare-earth ion size increases, due to the large increase of δ_a. Again, these results agree with the large variation rate of the shear-strain found in the $RMnO_3$, namely for the largest rare-earths.

The different behaviour found on the $RFeO_3$ and the $RMnO_3$ must be attributed to the Jahn-Teller distortion, since it is present in the latter but not in the former. This means that the Jahn-Teller distortion is in fact an important mechanism to accommodate hydrostatic pressure, being also the driving force for the anisotropic volume reduction. Moreover, we can also realize that this distortion is most probably the mechanism yielding the lack of a rule for the high-pressure phase symmetry of the $RMnO_3$, in contrast with the common isostructural one found in the $RFeO_3$. This interpretation is based on the fact that since the volume reduction of the $RFeO_3$ is close to isotropic, even though the octahedra tilts and shear-strain are not constant, the *Pnma* structure is not changed too much, and is still suitably stable to be maintained after the volume collapse at P_C. This explanation even predicts that $DyMnO_3$, the only $RMnO_3$ with variation rates of shear-strain within the range found for $RFeO_3$, would also maintain the *Pnma* symmetry above P_C, which in fact is observed. Contrarily, for the $RMnO_3$ from Gd to larger radius rare-earth ions that present a strong anisotropic volume reduction up to P_C, the *Pnma* structure becomes unstable at P_C, above which the system stabilizes in other more suitable symmetries. Thus, the symmetry of the high-pressure phase is different from the one of the low-pressure phase, and it depends on the degree of anisotropy of the volume reduction up to the transition pressure.

3 Conclusions

In this work, we have compared the structural evolution of $RFeO_3$ and $RMnO_3$ under applied hydrostatic pressure, from which the critical pressure of the insulator-to-metal phase transition was obtained, and the nature of the high-pressure phase symmetry discussed. We were able to conclude that the pressure accommodation in the $RMnO_3$ is much more anisotropic than in the $RFeO_3$, which is almost isotropic. This feature yields the shear-strain to change more drastically in the $RMnO_3$ than in the $RFeO_3$, though for both a crossover between an enhancement and a reduction of this strain occurs for R = Dy and Eu, respectively. The anisotropy of the volume reduction in the $RMnO_3$ may be responsible for the different high-pressure phase symmetries for different rare-earth ions, in contrast with the common isostructural phase transition of the $RFeO_3$. Since the Jahn-Teller distortion marks alone the structural difference between $RFeO_3$ and $RMnO_3$, the degree of the anisotropic compression can be apparently ascribed to the role played by that distortion.

References

1 J. Zhao, N.L. Ross, R.J. Angel, Acta Crystallogr. Sect. B Struct. Sci. **60**, 263 (2004)

2 H.J. Xiang, M. Guennou, J. Íñiguez, J. Kreisel, L. Bellaiche, Phys. Rev. B **96**, 054102 (2017)

3 P. Chen, M.N. Grisolia, H.J. Zhao, O.E. González-Vázquez, L. Bellaiche, M. Bibes, B.G. Liu, J. Íñiguez, Phys. Rev. B **97**, 024113 (2018)

4 J. Oliveira, J. Agostinho Moreira, A. Almeida, V. Rodrigues, M.M. Costa, P. Tavares, P. Bouvier, M. Guennou, J. Kreisel, Phys. Rev. B **85**, 052101 (2012)

5 D.A. Mota, A. Almeida, V.H. Rodrigues, M.M.R. Costa, P. Tavares, P. Bouvier, M. Guennou, J. Kreisel, J. Agostinho Moreira, Phys. Rev. B **90**, 054104 (2014)

6 R. Vilarinho, P. Bouvier, M. Guennou, I. Peral, M.C. Weber, P. Tavares, M. Mihalik, M. Mihalik, G. Garbarino, M. Mezouar, J. Kreisel, A. Almeida, J. Agostinho Moreira, Phys. Rev. B **99**, 064109 (2019)

7 H.J. Zhao, Y. Yang, W. Ren, A. Mao, J. Phys. Condens. Matter 472201 (2014).

8 J.-H. Lee, Y.K. Jeong, J.H. Park, M.-A. Oak, H.M. Jang, J.Y. Son, J.F. Scott, Phys. Rev. Lett. **107**, 117201 (2011)

9 A.G. Gavriliuk, G.N. Stepanov, I.S. Lyubutin, A.S. Stepin, I.A. Trojan, V.A. Sidorov, Hyperfine Interact. **126**, 305 (2000)

10 A.G. Gavriliuk, I.A. Troyan, R. Boehler, M.I. Eremets, I.S. Lyubutin, N.R. Serebryanaya, J. Exp. Theor. Phys. Lett. **77**, 619 (2003)

11 M. Baldini, V. V. Struzhkin, A.F. Goncharov, P. Postorino, W.L. Mao, Phys. Rev. Lett. **106**, 066402 (2011)

12 M.P. Pasternak, W.M. Xu, G.K. Rozenberg, R.D. Taylor, Mater. Res. Soc. Symp. Proc. **718**, D2.7.1 (2002)

13 M. Etter, M. Müller, M. Hanfland, R.E. Dinnebier, Acta Crystallogr. Sect. B Struct. Sci. Cryst. Eng. Mater. **70**, 452 (2014)

14 N.A. Halasa, G. Depasquali, H.G. Drickamer, Phys. Rev. B **10**, 154 (1974)

15 R. Vilarinho, D.J. Passos, E.C. Queirós, P.B. Tavares, A. Almeida, M.C. Weber, M. Guennou, J. Kreisel, J. Agostinho Moreira, Phys. Rev. B **97**, 144110 (2018)

16 M.A. Carpenter, B.A. I., S. Friedrich, Am. Mineral. **86**, 348 (2001)

17 M.A. Carpenter and C.J. Howard, Acta Crystallogr. Sect. B **65**, 134 (2009)